Computational Materials Science 154 (2018) 97–105

Contents lists available at ScienceDirect

Computational Materials Science

journal homepage: www.elsevier.com/locate/commatsci

A two-class rotation transmission nanobearing driven by gigahertz rotary nanomotor

Wei Qiu, Jiao Shi*, Zheng Cao, Jicheng Zhang, Ning Wei*

College of Water Resources and Architectural Engineering, Northwest A&F University, Yangling 712100, China

ARTICLE INFO

Keywords:
Nanomotor
Nanobearing
Transmission system
Carbon nanotube
Molecular dynamics

ABSTRACT

For a vehicle, its speed can be adjusted via a transmission system. In this study, we propose a model of two-class rotation transmission nanosystem to adjust the input rotation via a gigahertz rotary nanomotor. To obtain an efficient rotation transmission system, carbon nanotubes, which have super-high in-shell strength but extremely low inter-shell friction, are adopted to build the coaxially rotary components. Besides 200 GHz motor, the other two components are the rotor1 in the class-1 nanobearing, and the rotor2 in the class-2 bearing, respectively. Considering both the chirality and radii differences of the rotary components, 27 types of transmission models are built and tested via molecular dynamic simulations. When the transmission ratio of the rotational frequency of the rotor2 and the input frequency is between 0.1 and 0.9, a successful transmission system is obtained. According to the rotation transmission ratios (RTRs) of both rotors in each model, some conclusions are drawn for potential design of such nanodevice. Besides, temperature can also influence the output rotation of the rotor2. It implies another way to adjust the output rotation from the same transmission system.

1. Introduction

It is well known that the in-plane strength of graphene [1] is extremely high, ~130 GPa [2], and the inter-plane friction is slight. The reason is that the in-plane strength is determined by the strength of $2sp^2$-$2sp^2$ covalent bonds. And the inter-plane interaction during relative sliding between neighbor graphene layers mainly depends on the repulsion of delocalized π electrons of the carbon atoms. Carbon nanotube (CNT) [3], a type of one-dimensional carbon material, behaves similarly with graphene, i.e., very high in-shell strength but extremely low friction between neighbor shells [4–6]. With consideration of the two excellent mechanical properties, i.e., Carbon nanotubes are popular in design of nanodevices, such as, nanooscillator [7–10], nanobearing [11–14], nanomotor [15–23], etc.

For a rotary nanomotor, it can play as an engine to drive some nanodevices like machines [24]. The rotational frequency of the nanomotor is commonly beyond the requirement of the device. When the rotational frequency of the nanomotor is difficult to adjust directly, people have to introduce an extra component to meet the requirement. To obtain a specified rotational frequency from the nanomotor, like a transmission system in a car, a nanosystem is needed to transfer the input rotation from the nanomotor to the given output rotation. In 2015, Cai et al. [25,26] proposed the concept of rotation transmission system from carbon nanotubes to transfer both the magnitude and direction of the motor's rotation. In their model, a rotary CNT motor coaxially laid with a CNT nanobearing form into a nanosystem for rotation transmission. The rotor in the bearing is driven to rotate by the nanomotor via the interaction at their adjacent edges. Their results demonstrate that the output rotational frequency of the rotor in the nanobearing has large amplitude fluctuation when the bearing is made from armchair CNTs. Sudden drop of the output rotation happens frequently. Even using zigzag CNTs as the nanobearing, the output rotation still has obvious fluctuation. The reason is that the rotor in the bearing has degree of freedom along axial direction, and can oscillate during rotating. During oscillation, the gap between the neighbor edges of the motor and the rotor varies with time, and the interaction between them is not stable. This is the reason for the fluctuation of the rotor's rotational frequency.

To overcome the difficulty, and to obtain a frequency-reducing transmission system, in the present study, we introduce two-class rotation transmission system from carbon nanotubes as shown in Fig. 1. Comparing to the models in reference [25], the present model has two coaxial nanobearings, i.e., class-1 and class-2 bearings. The motion of rotor1 is constrained by more components, including both L-stators, the right edge of the motor, the R-stator1, and the rotor2. Hence, the oscillation of the rotor1 happens difficultly. To show the feasibility and

* Corresponding authors.
E-mail addresses: shijiaoau@163.com (J. Shi), nwei@nwsuaf.edu.cn (N. Wei).

https://doi.org/10.1016/j.commatsci.2018.07.030
Received 20 May 2018; Received in revised form 9 July 2018; Accepted 16 July 2018

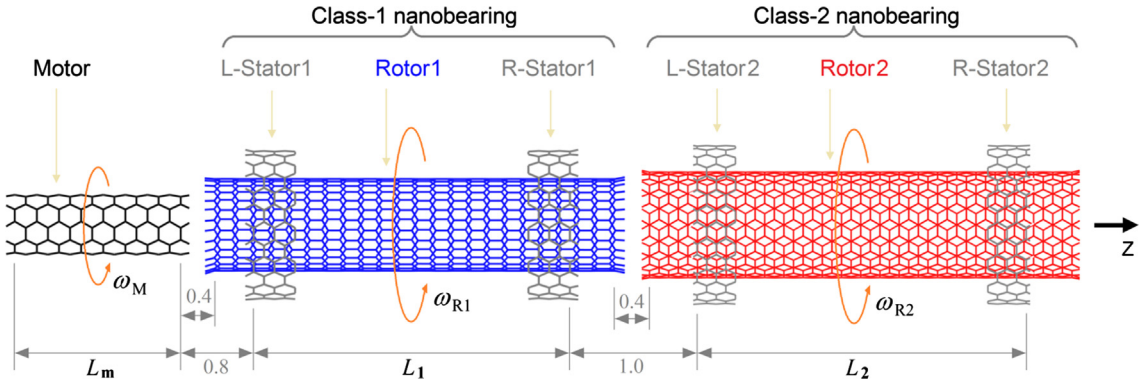

Fig. 1. Schematic of a two-class rotation transmission system (TCRTS) made from carbon nanotubes. It contains a motor with input rotation and two bearings from DWNTs (e.g., (5,5)/(10,10) with (5,5) as rotor and (10,10) as stators). All tube axes are aligned and all external ends of tubes are hydrogenated. The initial gap between the motor and the rotor1, or between both rotors, is 0.4 nm. Other geometric parameters of the system are listed in Tables 1 and 2. ω_M is the input rotational frequency of the motor. ω_{R1} and ω_{R2} are the output rotational frequencies of the rotor1 and the rotor2, respectively.

Table 1
Radii and lengths of CNTs as rotors in TCRTS involved in simulations. Dimension unit: nm.

CNT	(8,0)	(5,5)	(9,0)	(14,0)	(16,0)	(17,0)	(10,10)	(18,0)	(13,13)	(15,15)	(18,18)
Radius	0.313	0.339	0.353	0.548	0.627	0.665	0.678	0.703	0.881	1.017	1.221
Length	7.952	7.993	7.952	8.165			7.993		7.993		

Table 2
Geometric parameters of the 27 different TCRTS models involved in simulations.

(a) Both motor and rotor 1 from the same CNT. DWNTs (5,5)/(10, 10), (8,0)/(17,0), and (14,0)/(13,13) as bearings

Model No.	1	2	3	4	5	6	7	8	9
Motor	(5,5)	(5,5)	(5,5)	(8,0)	(8,0)	(8,0)	(14,0)	(14,0)	(14,0)
Rotor1	(5,5)	(5,5)	(5,5)	(8,0)	(8,0)	(8,0)	(14,0)	(14,0)	(14,0)
Rotor2	(5,5)	(8,0)	(14,0)	(5,5)	(8,0)	(14,0)	(5,5)	(8,0)	(14,0)
L_1/nm	7.225	7.193	7.193	7.152	7.152	7.152	7.365	7.365	7.365
L_2/nm	6.302	6.302	6.301	6.302	6.302	6.302	6.302	6.302	6.301
L_m/nm	3.074	3.074	3.074	2.840	2.840	2.840	3.053	3.053	3.053

(b) Both motor and rotor 2 from the same CNT. DWNTs (5,5)/(10, 10), (8,0)/(17,0), (9,0)/(18,0) and (14,0)/(13,13) as bearings

Model No.	10	11	12	13	14	15	16	17	18
Motor	(5,5)	(5,5)	(5,5)	(8,0)	(8,0)	(8,0)	(14,0)	(14,0)	(14,0)
Rotor1	(8,0)	(9,0)	(14,0)	(5,5)	(9,0)	(14,0)	(5,5)	(8,0)	(9,0)
Rotor2	(5,5)	(5,5)	(5,5)	(8,0)	(8,0)	(8, 0)	(14,0)	(14,0)	(14,0)
L_1/nm	7.152	7.152	7.365	7.194	7.152	7.365	7.193	7.152	7.152
L_2/nm	6.302	6.302	6.302	6.302	6.302	6.302	6.302	6.302	6.302
L_m/nm	3.074	3.074	3.074	2.840	2.840	2.840	3.053	3.053	3.053

(c) The motor, and both rotors are made from different CNTs

Model No.	19	20	21	22	23	24	25	26	27
Motor	(5,5)	(5,5)	(9,0)	(9,0)	(14,0)	(14,0)	(5,5)	(5,5)	(10,10)
Rotor1	(9,0)	(14,0)	(5,5)	(14,0)	(5,5)	(9,0)	(10,10)	(13,13)	(5,5)
Stator1	(18,0)	(13,13)	(10,10)	(13,13)	(10,10)	(18,0)	(15,15)	(18,18)	(10,10)
Rotor2	(14,0)	(9,0)	(14,0)	(5,5)	(9,0)	(5,5)	(13,13)	(10,10)	(13,13)
Stator2	(13,13)	(16,0)	(13,13)	(10,10)	(18,0)	(10,10)	(18,18)	(15,15)	(18,18)
L_1/nm	7.152	7.365	7.194	7.365	7.193	7.152	7.193	7.194	7.193
L_2/nm	6.302	6.302	6.302	6.302	6.302	6.302	6.302	6.302	6.302
L_m/nm	3.074	3.074	2.840	2.840	3.053	3.053	3.074	3.074	3.074

efficiency of rotation transmission, in this study, the input rotational frequency is set to be 200 GHz. Three other factors are considered in simulation. The first factor is the chirality of nanotubes in the rotary components. Besides, the radii difference is also considered. Detailed parameters are given in Table 1. The second factor is the layout of the nanotubes in the three components. Detailed schemes are listed in Table 2, and supporting materials. The final factor is the temperature of system. At higher temperature, the vibration of atoms in tubes is more drastic, and the interaction between neighbor edges of motor and rotors varies greater. Discussion on the dynamics response of the systems is in Section 3.

2. Model and methodology

2.1. Model of a two-class rotation transmission system

Fig. 1 gives the schematic of a two-class rotation transmission system. The components are made from CNTs. The parameters of the

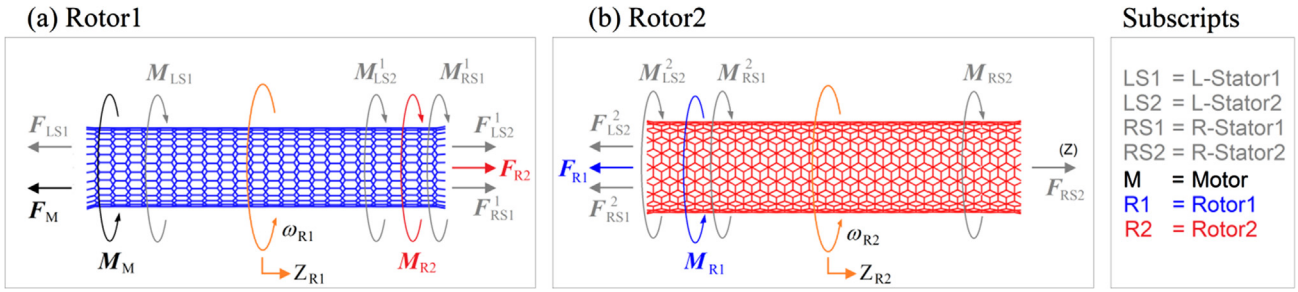

Fig. 2. Free body diagrams of both rotors in a rotation transmission system. (a) Rotor1 subjected to axial forces $\boldsymbol{F}_{\mathrm{M}}$, $\boldsymbol{F}_{\mathrm{LS1}}$, $\boldsymbol{F}^{1}_{\mathrm{LS2}}$, $\boldsymbol{F}^{1}_{\mathrm{RS1}}$, and $\boldsymbol{F}_{\mathrm{R2}}$, and axial torque moments $\boldsymbol{M}_{\mathrm{M}}$, $\boldsymbol{M}_{\mathrm{LS1}}$, $\boldsymbol{M}^{1}_{\mathrm{LS2}}$, $\boldsymbol{M}^{1}_{\mathrm{RS1}}$, and $\boldsymbol{M}_{\mathrm{R2}}$. (b) Rotor2 subjected to axial forces $\boldsymbol{F}_{\mathrm{R1}}$, $\boldsymbol{F}^{2}_{\mathrm{LS2}}$, $\boldsymbol{F}^{2}_{\mathrm{RS1}}$, and $\boldsymbol{F}_{\mathrm{RS2}}$, and axial torque moments $\boldsymbol{M}_{\mathrm{R1}}$, $\boldsymbol{M}^{2}_{\mathrm{LS2}}$, $\boldsymbol{M}^{2}_{\mathrm{RS1}}$, and $\boldsymbol{M}_{\mathrm{RS2}}$. Z_{R1} and Z_{R2} are mass centers of both rotors, respectively. $\boldsymbol{F}_{\mathrm{LS1}}$ means the friction from L-Stator1. $\boldsymbol{M}_{\mathrm{RS2}}$ represents the torque moment from R-Stator2. Similar definitions for other loading variables.

CNTs involved in models are listed in Table 1. And the chirality of the CNTs in the models is illustrated in Table 2. There are 27 models are built and tested. The configurations of the models can be found in Supporting Materials.

2.2. Method

(a) Free body diagrams of both rotors in a system

The forces and moments applied on both rotors are illustrated in Fig. 2. According to the law of action and reaction, $\boldsymbol{F}_{\mathrm{R1}} + \boldsymbol{F}_{\mathrm{R2}} = 0$; $\boldsymbol{M}_{\mathrm{R1}} + \boldsymbol{M}_{\mathrm{R2}} = 0$. $\boldsymbol{F}_{\mathrm{M}}$ means the van der Waals (vdW) force which is given by the motor. $\boldsymbol{M}_{\mathrm{M}}$ means the friction-induced torque moment given by the motor. The rest vectors with subscriptions have similar explanations as $\boldsymbol{F}_{\mathrm{M}}$ or $\boldsymbol{M}_{\mathrm{M}}$. Radial effects on both rotors are not discussed in this study. As the outer edge of each stator and the adjacent edges of rotary components are hydrogenated, i.e., each carbon atom is covalently bonded with a hydrogen atom. Thus, the edge carbon atoms are saturated, and hardly bonds with other carbon or hydrogen atoms at normal condition. The interaction among the atoms on neighbor components in a system belongs to non-bonding interaction, and is described using Lennard-Jones (L-J) potential [27].

Fig. 1 indicates that the motion of the tube edges is confined within 0.8 nm or 1.0 nm. Considering the edge barriers [28] of the stators, both rotors have no chance to escape from the stators on condition that their radii difference is less than 0.34 nm. Meanwhile, the axial gap between neighbor edges of motor and rotors are commonly less than 0.8 nm, which is less than 1.02 nm, i.e., the cutoff of L-J potential in this study. Hence, the direction of each axial force may change during simulation. But this has no influence on the results of free body diagram.

(b) Analysis of motions of rotors

The rotational frequency of both rotors can be calculated using the following equations, i.e.,

$$\omega_{\mathrm{R1}}(t) = \int_0^t \frac{M_{\mathrm{M}} - M_{\mathrm{R2}} - M_{\mathrm{LS1}} - M^{1}_{\mathrm{LS2}} - M^{1}_{\mathrm{RS1}}}{\sum_{n1} m_i [x_i^2(s) + y_i^2(s)]} \mathrm{d}s \tag{1a}$$

$$\omega_{\mathrm{R2}}(t) = \int_0^t \frac{M_{\mathrm{R1}} - M^{2}_{\mathrm{LS2}} - M^{2}_{\mathrm{RS1}} - M_{\mathrm{RS2}}}{\sum_{n2} m_i [x_i^2(s) + y_i^2(s)]} \mathrm{d}s \tag{1b}$$

The relations between the mass centers of tubes and the loads are as following,

$$\frac{\mathrm{d}\mathrm{Z}_{\mathrm{R1}}}{\mathrm{d}t} = \int_0^t \frac{-F_{\mathrm{M}} + F_{\mathrm{R2}} - F_{\mathrm{LS1}} + F^{1}_{\mathrm{LS2}} + F^{1}_{\mathrm{RS1}}}{\sum_{n1} m_i} \mathrm{d}s \tag{2b}$$

$$\frac{\mathrm{d}\mathrm{Z}_{\mathrm{R2}}}{\mathrm{d}t} = \int_0^t \frac{F_{\mathrm{RS2}} - F^{2}_{\mathrm{LS2}} - F^{2}_{\mathrm{RS1}} - F_{\mathrm{R1}}}{\sum_{n2} m_i} \mathrm{d}s \tag{2c}$$

where $n1$, and $n2$ are the number of atoms in the rotor1 and rotor2, respectively. m_i, x_i, and y_i are the mass, coordinates x and y, of atom i, respectively. The mass centers at time s can also be described as,

$$\mathrm{Z}_{\mathrm{R1}} = \frac{\sum_{n1} m_i \times z_i(s)}{\sum_{n1} m_i}; \quad \mathrm{Z}_{\mathrm{R2}} = \frac{\sum_{n2} m_i \times z_i(s)}{\sum_{n2} m_i} \tag{3}$$

(c) Rotation transmission ratios

To show the efficiency of the rotation transmission of both rotors in a system, rotational transmission ratios (RTR) are defined, i.e.,

$$R_1 = \frac{\omega_{\mathrm{R1}}}{\omega_{\mathrm{M}}}; \quad R_2 = \frac{\omega_{\mathrm{R2}}}{\omega_{\mathrm{M}}} \tag{4}$$

The efficiency of rotation transmission is classified into three levels, i.e.,

(i) Failed transmission: After 20 ns of rotation, if both rotors have RTR values being less than 0.1 (or higher than 0.9), the transmission is unacceptable. We judge that the transmission fails.
(ii) Available transmission: After 20 ns of rotation, if both values of RTR are between 0.1 and 0.9, the transmission is acceptable, and the system can provide an available frequent-reducing transmission.
(iii) Excellent transmission: After 20 ns of rotation, if both values of RTR are between 0.4 and 0.6.

According to the definition of RTR in Eq. (4), the values of RTR may be negative or higher than 1.0. If RTR is negative, the rotor rotates oppositely to the motor. If RTR is higher than 1.0, over-speeding state happens for the system [29].

(d) Details for MD simulations

Molecular dynamics simulations are used to exhibit the efficiency of rotation transmission of the systems in the models with detailed parameters listed in Tables 1 and 2. Simulations are fulfilled using the open-source code LAMMPS [30]. Interaction among carbon and hydrogen atoms is evaluated by AIREBO potential [31]. The time step is set to 0.001 ps. Maximum iteration is 20 million. The configuration of system is reshaped by minimization of potential of the system. After minimization, all tubes are partly fixed. For instance, the left 5 rings of carbon atoms, the left two rings of carbon atoms of each rotor, and all carbon atoms in each stator, are fixed. And the system is in thermal bath at NVT ensemble for 200,000 steps, i.e., 200 ps of simulation. After relaxation, the motor starts rotating with 200 GHz of frequency, and

both rotors are released of their fixed degrees of freedom (DOF), simultaneously. Solid boundaries are adopted in three dimensions. Each 200 steps of simulation results are averaged and the mean values are recorded for further analysis. The temperature is controlled using Nosé-Hoover thermostat [32].

The AIREBO potential contains three items, i.e.,

$$\begin{cases} P = P_{\mathrm{REBO}} + P_{\mathrm{Torsion}} + P_{\mathrm{L-J}} \\ P_{\mathrm{REBO}} = \sum_i \sum_{j(j>i)} [V_R(r_{ij}) - bij V_A(r_{ij})] \\ P_{\mathrm{Torsion}} = \frac{1}{2} \sum_i \sum_{j(j\neq i)} \sum_{k(k\neq i,j)} \sum_{l(l\neq i,j,k)} w_{ij}(r_{ij}) \cdot w_{jk}(r_{ij}) \cdot w_{kl}(r_{ij}) \cdot V_{\mathrm{T}}(\omega_{ijkl}) \\ P_{\mathrm{L-J}} = \sum_i \sum_{j(j>i)} 4\varepsilon_{ij} \left[\left(\frac{\sigma_{ij}}{r_{ij}} \right)^{12} - \left(\frac{\sigma_{ij}}{r_{ij}} \right)^{6} \right] \end{cases} \tag{5}$$

where P_{REBO} is the REBO potential to describe the short-range bonding interaction. Parameters V_R and V_A are repulsive and attractive parts between atoms i and j with distance of r_{ij}, and b_{ij} is the bond-order term. P_{Torsion} is the potential due to the change of dihedral angle ω of the neighbor atoms i, j, k, and l. Bond weight satisfies $1.0 \geq w_{ij} \geq 0$. $P_{\mathrm{L-J}}$, i.e., L-J potential describes the non-bonding interaction, with $\sigma_{\mathrm{C-C}} = 0.34$ nm, $\sigma_{\mathrm{H-H}} = 0.265$ nm, $\sigma_{\mathrm{C-H}} = (\sigma_{\mathrm{C-C}} + \sigma_{\mathrm{H-H}})/2$, $\varepsilon_{\mathrm{C-C}} = 2.84$ meV, $\varepsilon_{\mathrm{H-H}} = 1.5$ meV, $\varepsilon_{\mathrm{C-H}} = 1.376$ meV.

3. Results from simulations and discussion

3.1. Motor and rotor1 having the same chirality

For the rotation transmission models in M1–M9, both the motor and the rotor1 have the same chirality of their CNTs. If the rotor2 in one of the nine models can give a nice output rotation, the motor and the rotor can be fabricated by tailing a CNT at their adjacent edges with consideration of the relative position of the L-stator1 to the motor. To show the rotation transmission effect, we give the RTR curves of the rotors in the nine models in Fig. 3.

For the first three models, i.e., M1, M2, and M3, they have the same motor and the same rotor1 (see the first row in Fig. 3). One can find that both rotors in M1 or M2 rotate synchronously with the motor after 10 ns. Due to the rotor2, i.e., (5,5) CNT in M1, being constrained by armchair stators which provide higher friction on the rotor2 (Table 2a), the values of RTR of both rotors are ~0.4 before 9 ns. In M2, the rotor2 is made from (8,0) CNT which is constrained by the zigzag stators. Hence, both rotors rotate synchronously with the motor soon after releasing their DOF constraints. When the rotor2 is made from a zigzag CNT with radius much higher than that of (8,0) CNT, we find that the rotor2, i.e., (14,0) CNT in M3 is not rotating synchronously with the rotor1 even after 20 ns. Two major reasons cause this phenomenon. One is that, when they are layout concentrically, their adjacent hydrogenated ends have strong vdW interaction [25]. The other is that the left edge of the rotor1 is constrained within 0.8 nm between the right edge of motor and the left edge of the L-stator1 (see Fig. 1). From the final values of RTR of both rotors in the three models, one can conclude that using the same armchair CNT as motor and rotor1, the transmission system fails to give a stable output which is different from the input via the motor.

For the three models, i.e., M4–M6, both of the motor and the rotor1 are made from the same zigzag CNT. By observing the curves of transmission ratio of the rotors as shown in Fig. 3, we find that the rotor1 always rotate synchronously with the motor within 2 ns. If the rotor2 is also made from the zigzag CNT, e.g., in M5, M6, M8 or M9, the final value of RTR of the rotor2 is slightly different from 1.0, which means that the transmission fails. If the rotor2 is from armchair CNT, e.g., (5,5) in M4 or M7, the final value of RTR of the rotor2 is obviously different from 1.0. For example, the final stable value of RTR of the rotor2 in M4 is ~0.81, which is much higher than 0.41 of the rotor2 in M7. The reason is that the radii difference between both rotors, i.e., (8,0) and (5,5) CNTs, in M4 is smaller than that in M7. Smaller radii difference means stronger edge interaction. Hence, one can design a two-class rotation transmission system by using a zigzag CNT as the rotor1 and an armchair CNT as the rotor2. The output rotation depends on their radii difference.

Beyond giving the above discussion, two phenomena are worthy of demonstration. One is the curvature of the rotor1 during rotating. In the system in M6, the difference between both ratios is ~0.1 when the rotors have stable rotation. From the initial and final configurations of

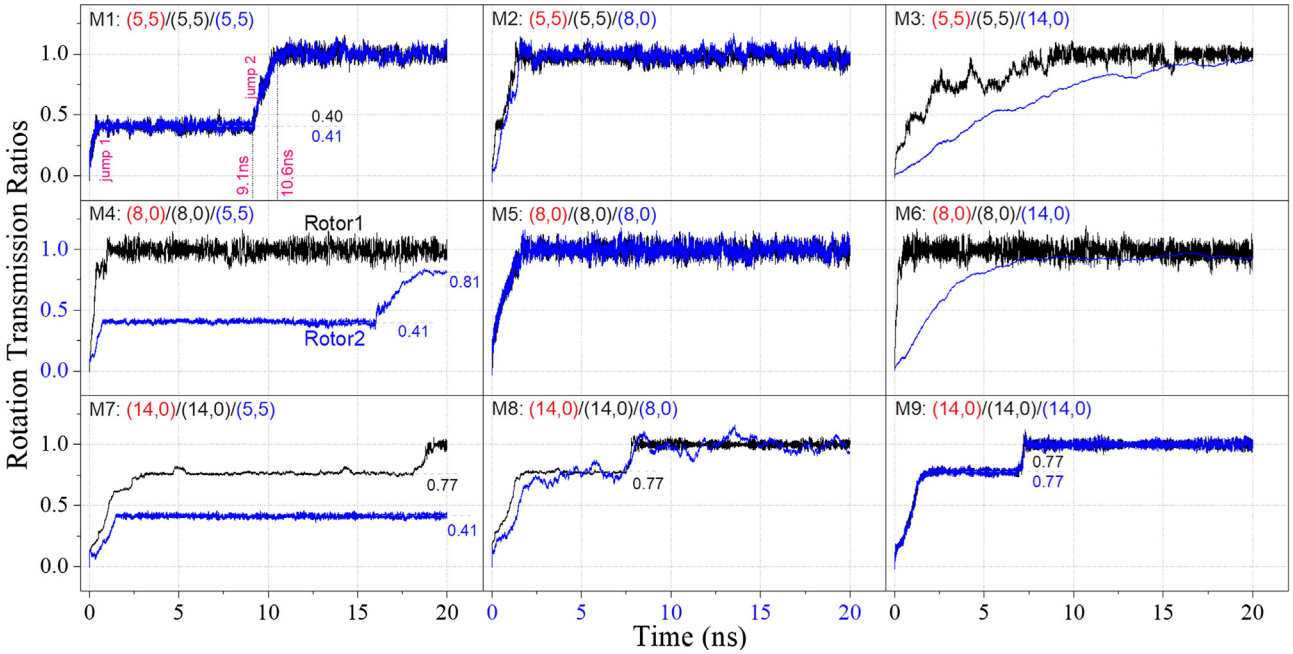

Fig. 3. Rotation transmission ratios of both rotors driven by the motors with 200 GHz of input frequency at 300 K. M1–M9 means Model No. 1–Model No. 9 with detailed parameters listed in Tables 1 and 2. M2: (5,5)/(5,5)/(8,0) means both motor and rotor1 are made from (5,5) CNT, rotor2 from (8,0) CNT. In each case, black and blue curves represent the ratios of the rotor1, and rotor2, respectively.

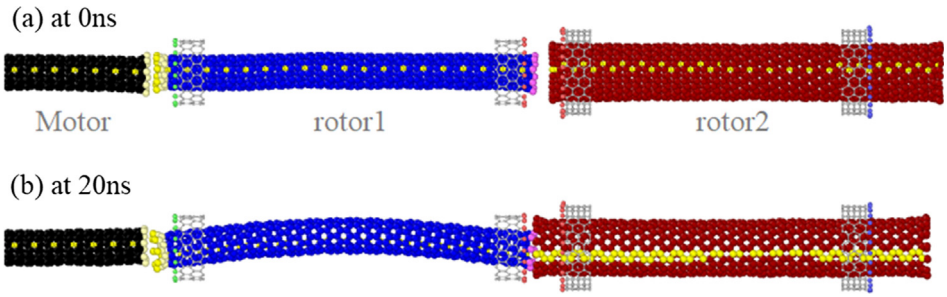

Fig. 4. Initial and final configurations of the system in M6 at 300 K. Black tube is the motor. Blue tube plays as the rotor1, and the red tube as the rotor2, respectively.

the system, the rotor1 is curved obviously (see Fig. 4). The curved tube, i.e., the rotor1, rotates synchronously with the motor. But the rotor2 does not keep the same step with the rotor1 because of the lower vdW interaction at their adjacent non-coaxial edges. Once reducing the initial length of the rotor1, the transversal bending can be avoided during rotating.

The other phenomenon is that the second jump up of the rotational speed of both rotors in M1, M8 or M9. For the rotors driven by the motor in M1 or M9, they have synchronous responses during rotating. For example, the first jump of their rotational speeds happens within the first 2 ns. After few nanoseconds of rotation with stable speeds lower than that of the motor, the second jump happens, and they are finally rotating synchronously with the motor. The response difference between the rotors in M1 and M9 is that the armchair rotors in M1 rotate slower than the zigzag rotors in M9 between two acceleration stages. The reason is that the potential barriers of the armchair CNT distribute uniformly in generatrix direction, but those of the zigzag CNT in circumferential direction [33]. Therefore, armchair stators in M1 provide higher friction on the related rotors than the zigzag stators in M9. During each jump, both rotors have drastic axial oscillation (Fig. 5). For example, both rotors in M1 have drastic axial oscillation during [9.1, 10.6]ns, in which their rotational speeds increase quickly (Fig. 3). When the oscillation disappears, both rotors rotate synchronously with the motor.

3.2. Motor and rotor2 having the same chirality

Different from the first nine models, in the models from M10 to M18, the motor and the rotor2 have the same chirality of their tubes. Between the two tubes, one can put the first-class nanobearing from different CNTs. If the output rotation of the rotor2 is obviously different from the input rotation via the motor, a successful frequent-reducing transmission system is obtained to give a different output rotation via the same CNT as that in the motor. To show the rotation transmission effect, the curves of RTR are shown in Fig. 6.

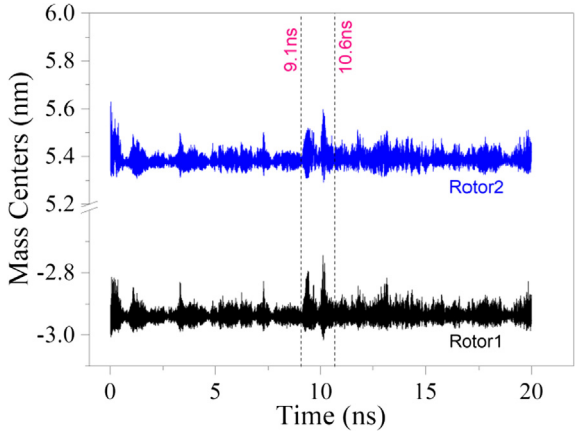

Fig. 5. History curves of mass centers of both rotors in M1 during rotating. Black curve represents the rotor1, and blue curve represents the rotor2.

When using (5,5) CNT to fabricate the motor and the rotor2, e.g., in M10, M11, and M12 (see the top row in Fig. 6), the output rotation of the rotor2 depends on the chirality of the CNTs in the first-class nanobearing. For example, in M10 with (8,0) CNT as the rotor1, the values of RTR of both rotors are less than 1.0, which indicates that both rotors rotates slower than the motor (Movie 1). If (9,0) CNT plays as the rotor1, both rotors almost rotate synchronously with the motor. The reason is that the (9,0) rotor1 provides stronger interaction on the rotor2 because of the radii difference between (5,5) and (9,0) CNTs being lower than that between (5,5) and (8,0) CNTs. When a zigzag CNT with radius higher than (5,5) CNT is used as the rotor1, e.g., (14,0) CNT in M12, the values of RTR of both rotors are much different from each other, and are also far less than 1.0. It means that the systems in M12 can effectively transfer the input rotation via the motor into a different out rotation of the rotor2.

In the models from M13 to M18 (the middle and the bottom rows in Fig. 6), the zigzag CNTs, e.g., (8,0) and (14,0) CNTs, are used to build the motor and the rotor2. When the (5,5) or (9,0) CNT is used as the rotor1, both rotors will finally rotate synchronously with the motor. It means that rotation transmission fails. When a CNT with higher radius as the rotor1, e.g., (14,0) CNT in M15, the output rotation of the rotor2 is ~0.66 which is much less than 1.0. Hence, M15 gives a successful transmission system. Accordingly, M16–M18 also suggest successful transmission system because of the final values of RTR of the rotor2 are ~0.78, ~0.58, and ~0.78, respectively. The rotor2 in M17 rotates slower than that in either M16 or M18 is due to the radii difference between both rotors is higher. Hence, we conclude that a successful frequent-reducing transmission system can be obtained when the radii difference between the rotor1 and the other two rotary components is higher than 0.18 nm (Table 1).

3.3. Motor and rotors having different chirality

From the response of the rotors in M12, M15, and M18, we know that the output rotation of the rotor2 is stable is much less than 1.0. Briefly, the three models provide a way to design an available transmission system from the CNTs with different radii. Now, we choose (5,5), (9,0), and (14,0) CNTs as the rotary components of a transmission system. Six different models, i.e., M19–M24, are built, and the rotors' rotation can be demonstrated by the RTR curves as shown in the top two rows in Fig. 7.

If the (14,0) CNT as the rotor2 (in M19 and M21), the output rotation is stable and the value of RTR of the rotor2 is ~0.83. The system from both M19 and M21 are available. When the rotor2 is made from (5,5) CNT (M22 and M24), both rotors have excellent outputs because the outputs are much less than those of M19 or M21. Especially, the values of RTR of each rotor in both models are different slightly. It means that the armchair CNT as the rotor2 can reduce the input rotational speed more efficient than the zigzag rotor2.

If the (9,0) CNT acts as the rotor2 (in M20 or M23), rotation

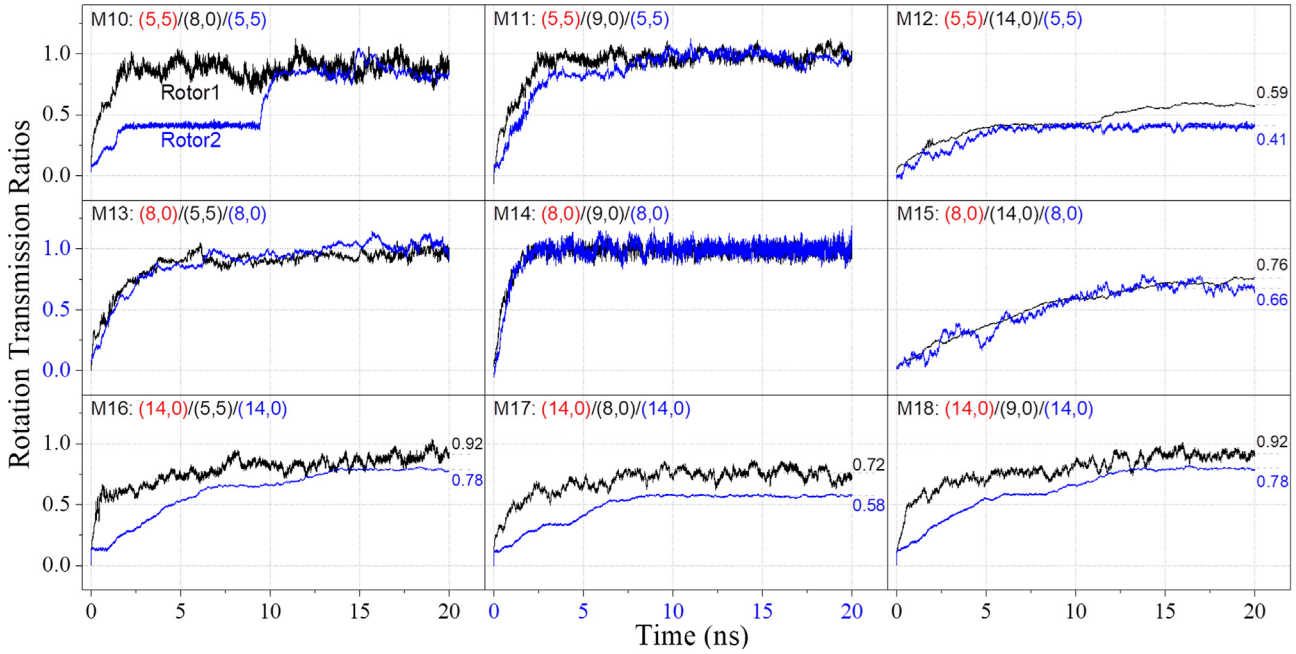

Fig. 6. Rotation transmission ratios of both rotors driven by the motors with 200 GHz of input frequency at 300 K. M10–M18 means Model No. 10–Model No. 18 with detailed parameters listed in Tables 1 and 2. In each case, black and blue curves represent the ratios of the rotor1, and rotor2, respectively.

transmission fails. For example, in M23, both rotors rotate synchronously with the motor. In M20, rotation of both rotors is far slower than the motor. From the snapshots in Fig. 8, one can find that the initial distance between the motor and the rotor1 is very small, it means that the interaction between them is stronger than that between both rotors. However, after 1000 ps of rotation, the rotor1 is attracted by the rotor2, and the motor provides lower driving force at the left edge of the rotor1. By comparing the relative positions of the rotary components at 1000 ps and 10,000 ps, we find that the rotor1 should be attracted by both the rotor2 and the R-Stator1 simultaneously. The reason is that when only the rotor2 provides attraction on the rotor1, both rotors still can oscillate along tube axis. But this does not happen. Also due to the interaction between the rotor1 and the R-Stator1, both rotors is more difficult to be driven by the motor. As a result, the system fails to give an available rotation transmission.

When all of the rotary components in a transmission system are made from armchair CNTs with different radii, e.g., (5,5), (10,10) and (13,13), rotation transmission of the system may fails when adjacent tubes have radii difference higher than 0.34 nm. For example, in M26, the (5,5) motor and the (13,13) rotor1 have radii difference of ~0.54 nm (> 0.34 nm), both rotors' rotational speed is far less than that of the motor. Because the rotor1 only can obtain slight rotational acceleration by the thinner motor, and therefore the rotor2 has slight rotational speed, either. In M27, the (5,5) and (13,13) CNTs are as both

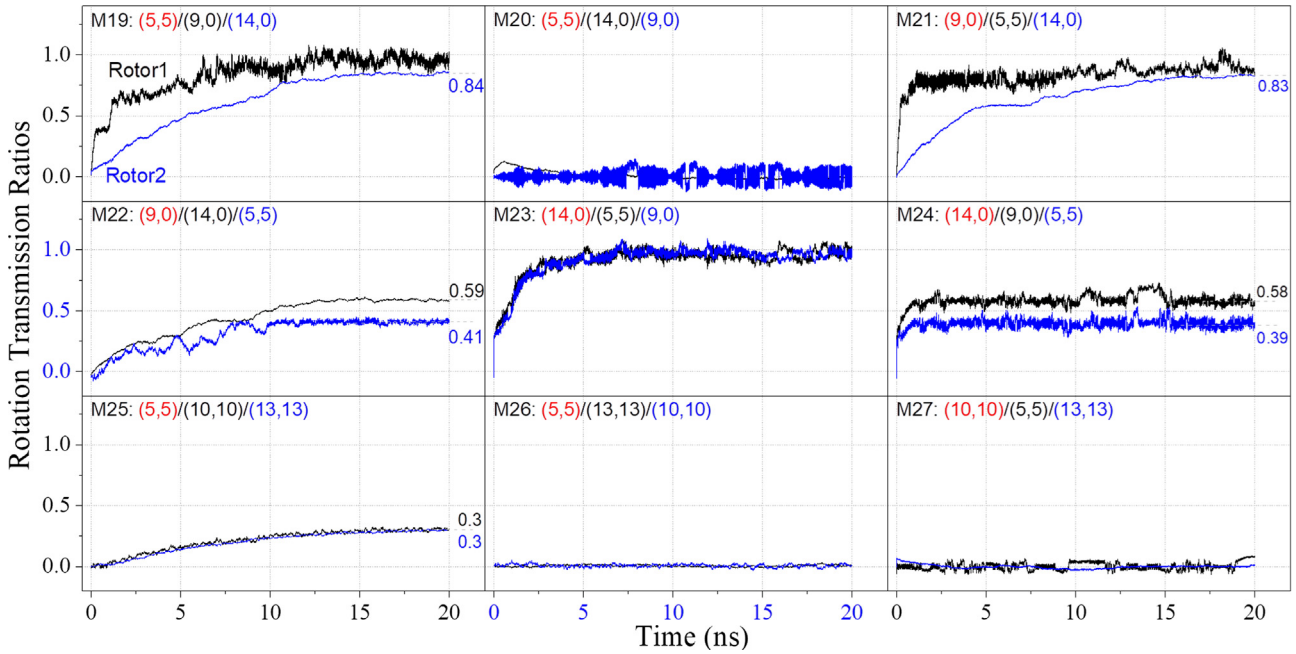

Fig. 7. Rotation transmission ratios of both rotors driven by the motors with 200 GHz of input frequency at 300 K. M19–M27 means Model No. 19–Model No. 27 with detailed parameters listed in Tables 1 and 2. In each case, black and blue curves represent the ratios of the rotor1, and rotor2, respectively.

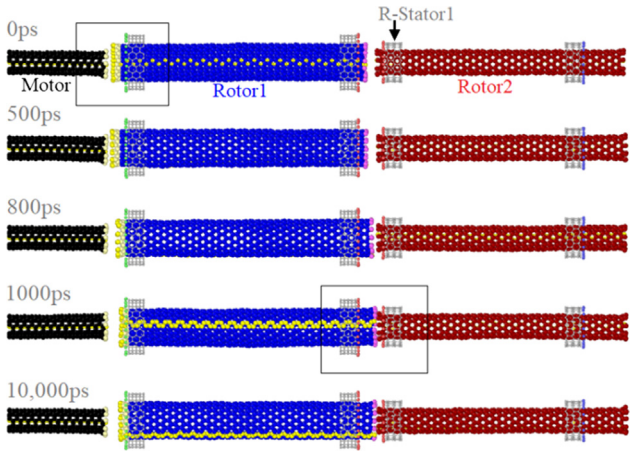

Fig. 8. Snapshots of the system in (5,5)/(14,0)/(9,0) model, i.e., M20 at 300 K.

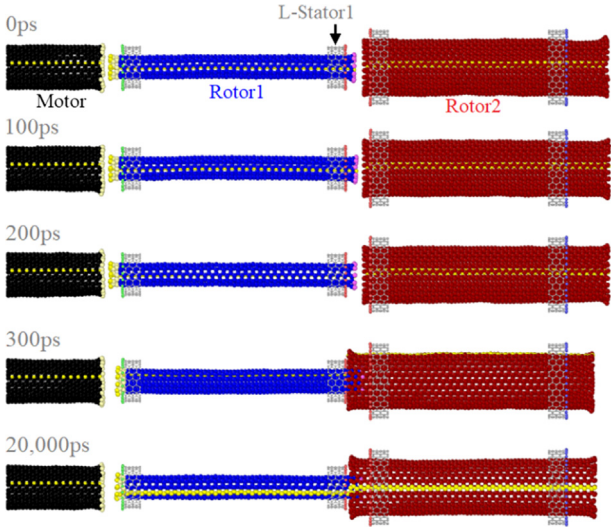

Fig. 9. Snapshots of the system in (10,10)/(5,5)/(13,13) model, i.e., M27 at 300 K.

rotors. Rotation of the (5,5) rotor1 hardly increases due to the radii difference between (5,5) and (10,10) CNTs is ~0.34 nm. From the snapshots of the system in M27 as shown in Fig. 9, the rotor2 is attracted by the L-Stator1, and does not move along the axis since 300 ps. Meanwhile, the right end of the (5,5) rotor1 enters into the (13,13) rotor2. Hence, the (13,13) CNT as the rotor2 is not driven to rotate, and transmission also fails.

3.4. Temperature effect

(a) Response of the systems in M23 and M25

As shown in Fig. 7, the difference between the RTR of both rotors in M23 or M25 is very small. In particular, both rotors in M23 are almost rotating synchronously with the motor at 300 K. To obtain a better output rotation of the rotor2, changing the temperature of system might be an approach. Here, four temperatures, i.e., 8 K, 100 K, 300 K, and 500 K, are involved in tests. The rotation transmission of the rotors in both models can be described by the curved in Fig. 10.

From both Fig. 10 and Table 3, one can find that the output rotation of the rotor2 depends on the temperature. For example, at 100 K or lower temperature, the mean value of RTR of the rotor2 is near 0.8. It means that rotation transmission is available for M23 at low temperature. At 300 K, the mean value of RTR of the rotor2 is ~0.956, which is slightly different from 1.0. Hence, rotation transmission of the same system at room temperature fails. At 500 K, the system does not in stable state before 6 ns. From the snapshots shown in Fig. 11, the motor tube and the rotor2 tube are damaged, and some carbon atoms escape from the tube before 4300 ps. The reason is that the tube's strength is lower at higher temperature and/or higher centrifugal force. And the rotor1 is curved during this period of ration. This is the reason for the sharp variation of the rotational speed of both rotors in M23 at 500 K during [2.5, 6]ns.

By putting the system in M25 at different temperatures, we find that the output rotational speed increases with the temperature. At the temperature lower than 100 K, both armchair rotors rotate synchronously (Table 3). At higher temperature, the rotational speeds of both rotors have small difference. From this phenomenon, we conclude that the difference of rotational speeds of both rotors in M25 cannot be enlarged by changing temperature.

(b) Response of the systems in M22 and M24

In Fig. 7, the curves of RTR of the rotors in M22 and M24 indicate that the two systems can provide excellent rotation transmission at 300 K. Now, we want to reveal the availability of the systems at very low temperature, e.g., between 5 K and 50 K. Fig. 12 shows the response of the rotors during rotation transmission.

The output rotation of the rotor2 depends on temperature. The maximum value of RTR happens at 5 K for each system. In M22, the rotor1 rotates slower than the rotor2 at 50 K at 20 ns. But obviously,

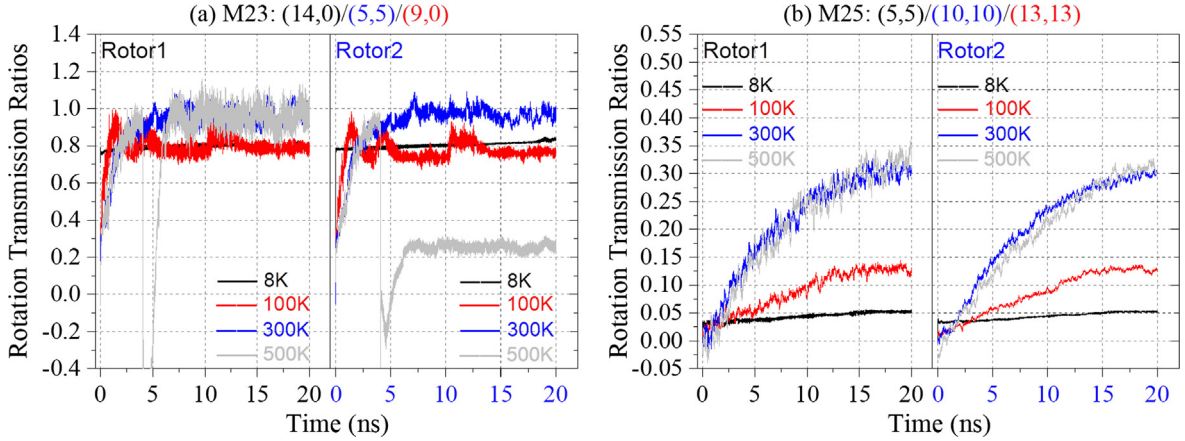

Fig. 10. History curves of RTR of both rotors in different models at temperature between 8 K and 50 K. (a) Rotors in M23, (b) rotors in M25. The input rotational frequency of motor is 200 GHz.

Table 3
Statistics results of RTR of rotors within [15, 20]ns at different temperatures. SD means standard deviation.

Model component		8 K		100 K		300 K		500 K	
		Mean	SD	Mean	SD	Mean	SD	Mean	SD
M23	Rotor1	0.804	0.005	0.788	0.017	0.972	0.048	0.957	0.053
	Rotor2	0.821	0.008	0.763	0.014	0.956	0.030	0.255	0.020
M25	Rotor1	0.052	0.002	0.128	0.005	0.301	0.011	0.314	0.018
	Rotor2	0.052	0.001	0.128	0.004	0.292	0.008	0.303	0.017

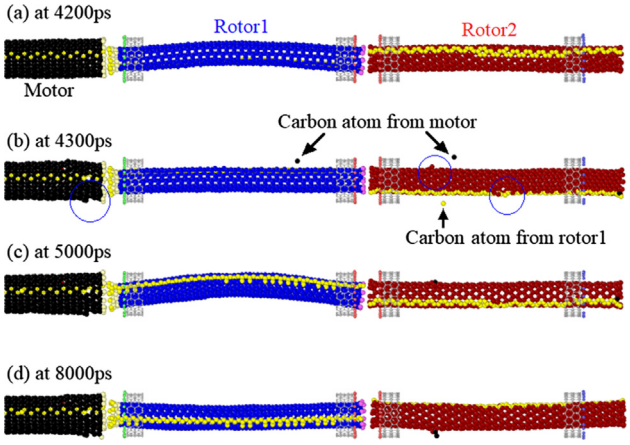

Fig. 11. Snapshots of the system in (14,0)/(5,5)/(9,0) model, i.e., M23 at 500 K.

both values of RTR of the rotors are no more than 0.2 (see pink curves in Fig. 12a). Fig. 7 has let us know that the values of RTR are between 0.4 and 0.6 at 300 K. Hence, after a longer time of driving by the motor, the rotor1 can rotates faster than the rotor2. For the rotors in M24, their rotational speed decreases with the temperature between 5 K and 30 K. Besides, from Table 4, one can find that the difference of RTR between both rotors is higher than 0.15. Hence, based on M24 one can design a rotation transmission system whose output rotation can be adjusted efficiently by changing temperature between 5 K and 30 K.

4. Conclusions

To obtain an efficient rotation transmission system from carbon nanotubes (CNTs), we test 27 types of 2-class transmission systems which have different nanotubes as rotary components. According to the rotation transmission ratios (RTRs) of both rotors driven by the 200 GHz motor, some conclusions as following can be drawn for potential design of such nanodevice, i.e.,

(i) Due to armchair stators providing stronger friction on the armchair rotor, the armchair rotor2 can reduce the output rotation more efficient than the zigzag rotor2.
(ii) When the same armchair CNT is used as motor and rotor1 in the class-1 bearing, the rotor2 in the class-2 bearing fails to give a lower stable output than the input via the motor.
(iii) If a zigzag CNT is used as the rotor1 and an armchair CNT as the rotor2, the output rotation depends on their radii difference. When radii difference between both rotors is higher than 0.18 nm, but less than 0.34 nm, the value of RTR of the rotor2 is between 0.1 and 0.9.
(iv) Using the same zigzag CNT as the motor and the rotor2, a successful frequent-reducing transmission system can be obtained when the rotor1 has lower radius than the motor.
(v) A successful frequent-reducing transmission system can be obtained when the radii difference between the rotor1 and the other two rotary components is higher than 0.18 nm. In this case, the motor and the rotor2 may have different radii, too.
(vi) Temperature is essential to the output rotation of the rotor2. For the same transmission system, e.g., in M25, its output rotational speed increases with the temperature between 8 K and 300 K, or in M24, the output rotation decreases with the increasing of temperature between 5 K and 50 K.

In the present study, the gap between the motor and the L-stator1, or between the L-stator2 and the R-stator1, is not involved. Actually, the interaction between neighbor rotary components is sensitive to both gaps. The influence of the gaps on the output rotation will be studied in near future.

Authors' contributions

W. Q. Built models and collect simulation data. J. S. wrote

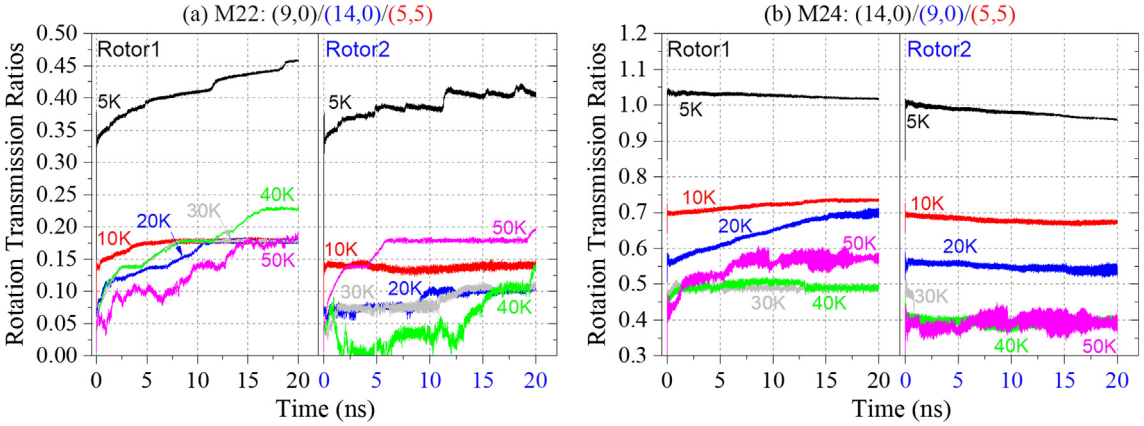

Fig. 12. History curves of RTR of both rotors in different models at temperature between 5 K and 50 K. (a) Rotors in M22, (b) rotors in M24. The input rotational frequency of motor is 200 GHz.

Table 4
Mean values of RTR of rotors within [19.5, 20]ns at different temperatures.

Model component		5 K	10 K	20 K	30 K	40 K	50 K
M22	Rotor1	0.458	0.179	0.178	0.178	0.228	0.184
	Rotor2	0.406	0.140	0.105	0.107	0.130	0.193
M24	Rotor1	1.018	0.735	0.699	0.489	0.490	0.572
	Rotor2	0.961	0.674	0.541	0.402	0.400	0.400

manuscript and gave analysis of data. Z. C. and J. Z. built models. N. W. gave data analysis and revision of manuscript.

Acknowledgements

The authors are grateful for financial support from National Key Research and Development Plan, China (Grant No.: 2017YFC0405102), National Natural Science Foundation, China (51505388, 11502217), Research Foundation for PhD in Northwest A&F University (Grant No.: 2452016176), Fundamental Research Funds for the Central Universities. China Postdoctoral Science Foundation (No. 2015M570854 and 2016T90949), HPC of NWAFU, the Youth Training Project of Northwest A&F University (No. Z109021600).

Appendix A. Supplementary material

Supplementary data associated with this article can be found, in the online version, at https://doi.org/10.1016/j.commatsci.2018.07.030.

References

[1] K.S. Novoselov, A.K. Geim, S.V. Morozov, et al., Electric field effect in atomically thin carbon films, Science 306 (5696) (2004) 666–669.
[2] C. Lee, X. Wei, J.W. Kysar, J. Hone, Measurement of the elastic properties and intrinsic strength of monolayer graphene, Science 321 (5887) (2008) 385–388.
[3] S. Iijima, Helical microtubules of graphitic carbon, Nature 354 (6348) (1991) 56–58.
[4] J. Cumings, A. Zettl, Low-friction nanoscale linear bearing realized from multiwall carbon nanotubes, Science 289 (2000) 602–604.
[5] R. Zhang, et al., Superlubricity in centimetres-long double-walled carbon nanotubes under ambient conditions, Nat. Nanotechnol. 8 (12) (2013) 912–916.
[6] E.H. Cook, M.J. Buehler, Z.S. Spakovszky, Mechanism of friction in rotating carbon nanotube bearings, J. Mech. Phys. Solids 61 (2) (2013) 652–673.
[7] Q. Zheng, Q. Jiang, Multiwalled carbon nanotubes as gigahertz oscillators, Phys. Rev. Lett. 88 (4) (2002) 045503.
[8] S.B. Legoas, V.R. Coluci, S.F. Braga, et al., Molecular-dynamics simulations of carbon nanotubes as gigahertz oscillators, Phys. Rev. Lett. 90 (5) (2003) 055504.
[9] W.L. Guo, Y.F. Guo, et al., Energy dissipation in gigahertz oscillators from multi-walled carbon nanotubes, Phys. Rev. Lett. 91 (12) (2003) 125501.
[10] K. Cai, H. Yin, Q.H. Qin, Y. Li, Self-excited oscillation of rotating double-walled carbon nanotubes, Nano Lett. 14 (4) (2014) 2558–2562.
[11] B. Bourlon, D.C. Glattli, C. Miko, et al., Carbon nanotube based bearing for rotational motions, Nano Lett. 4 (2004) 709–712.
[12] V.V. Deshpande, H.Y. Chiu, H.W.C. Postma, et al., Carbon nanotube linear bearing nanoswitches, Nano Lett. 6 (2006) 1092–1095.
[13] C. Zhu, W. Guo, T. Yu, Energy dissipation of high-speed nanobearings from double-walled carbon nanotubes, Nanotechnology 19 (2008) 465703.
[14] J. Shi, K. Cai, L.N. Liu, Q.H. Qin, Conditions for escape of a rotor in a rotary nanobearing from short triple-wall nanotubes, Sci. Rep. 8 (2018) 913.
[15] A. Fennimore, T. Yuzvinsky, W.Q. Han, et al., Rotational actuators based on carbon nanotubes, Nature 424 (2003) 408–410.
[16] J.W. Kang, H.J. Hwang, Nanoscale carbon nanotube motor schematics and simulations for micro-electro-mechanical machines, Nanotechnology 15 (2004) 1633–1638.
[17] Z.C. Tu, X. Hu, Molecular motor constructed from a double-walled carbon nanotube driven by axially varying voltage, Phys. Rev. B 72 (2005) 033404.
[18] B. Wang, L. Vuković, P. Král, Nanoscale rotary motors driven by electron tunneling, Phys. Rev. Lett. 101 (18) (2008) 186808.
[19] A. Barreiro, R. Rurali, E.R. Hernandez, et al., Subnanometer motion of cargoes driven by thermal gradients along carbon nanotubes, Science 320 (2008) 775–778.
[20] H.A. Zambrano, J.H. Walther, R.L. Jaffe, Thermally driven molecular linear motors: a molecular dynamics study, J. Chem. Phys. 131 (24) (2009) 241104.
[21] M. Hamdi, et al., Simulation of rotary motion generated by head-to-head carbon nanotube shuttles, Mech., IEEE/ASME Trans. 18 (1) (2013) 130–137.
[22] K. Cai, J.Z. Yu, J. Wan, et al., Configuration jumps of rotor in a nanomotor from carbon nanostructures, Carbon 101 (2016) 168–176.
[23] K. Cai, J.Z. Yu, et al., Rotation measurements of a thermally driven rotary nanomotor with a spring wing, Phys. Chem. Chem. Phys. 18 (2016) 22478–22486.
[24] http://www.nobelprize.org/nobel_prizes/chemistry/laureates/2016/press.html, 2016 [cited 2018 20 March].
[25] K. Cai, H. Yin, N. Wei, et al., A stable high-speed rotational transmission system based on nanotubes, Appl. Phys. Lett. 106 (2015) 021909.
[26] K. Cai, H.F. Cai, J. Shi, et al., A nano universal joint made from curved double-walled carbon nanotubes, Appl. Phys. Lett. 106 (2015) 241907.
[27] J.E. Jones, On the determination of molecular fields: II. From the equation of state of a gas, Proc. Royal Soc. London 106 (1924) 463–477.
[28] Z. Guo, T. Chang, X. Guo, H. Gao, Thermal-induced edge barriers and forces in interlayer interaction of concentric carbon nanotubes, Phys. Rev. Lett. 107 (2011) 105502.
[29] K. Cai, H.F. Cai, L. Ren, et al., Over-speeding rotational transmission of a carbon nanotube-based bearing, J. Phys. Chem. – C 120 (2016) 5797–5803.
[30] S. Plimpton, Fast parallel algorithms for short-range molecular dynamics, J. Comput. Phys. 117 (1) (1995) 1–19.
[31] S.J. Stuart, A.B. Tutein, J.A. Harrison, A reactive potential for hydrocarbons with intermolecular interactions, J. Chem. Phys. 112 (14) (2000) 6472–6486.
[32] S. Nosé, A molecular dynamics method for simulations in the canonical ensemble, Mol. Phys. 52 (1984) 255–268.
[33] R. Saito, R. Matsuo, T. Kimura, et al., Anomalous potential barrier of double-wall carbon nanotube, Chem. Phys. Lett. 348 (2001) 187–193.